Ku-Band InGaP–GaAs HBT MMIC VCOs With Balanced and Differential Topologies

Donghyun Baek, *Student Member, IEEE*, Sangsoo Ko, *Student Member, IEEE*, Jeong-Geun Kim, *Student Member, IEEE*, Dong-Wook Kim, and Songcheol Hong, *Member, IEEE*

***Abstract*—Balanced and differential voltage controlled oscillators (VCOs) are investigated with analytic noise models. Fully integrated VCOs in Ku-band are implemented on an InGaP–GaAs heterojunction bipolar transistor technology. The balanced VCO has higher output power and lower phase-noise performance, while drawing lower current than the differential VCO. This coincides with the analytical expectation. The shot noise of collector current contributes less to the phase noise in the balanced VCO (B-VCO) than in the differential VCO. The B-VCO shows 2–3 dB lower phase-noise performances of 90.5, −113.8 dBc/Hz at the offset frequencies 100 kHz, and 1-MHz offset at 13.5 GHz than the differential VCO, and figures of merit of 180.7 and −177.6 dBc/Hz are achieved, respectively.**

***Index Terms*—Differential and balanced topology, heterojunction bipolar transistor (HBT), inductor, InGaP–GaAs, monolithic microwave integrated circuit (MMIC), phase noise, voltage-controlled oscillator (VCO).**

I. Introduction

A VOLTAGE-CONTROLLED oscillator (VCO) is one of the most important building blocks in communication transceivers. Many research efforts have been devoted to fully integrated VCOs in 0.8–2.5 GHz for mobile communication systems such as personal communications systems (PCSs), global systems for mobile communications (GSMs), IMT2000, and 5–6 GHz for wireless local area networks (LANs) (UNII band) and high-performance LAN (HYPERLAN). Recently, VCOs that cover over 10-GHz hold a key post in areas of satellite communications, local multipoint distribution services (LMDSs), wide-band LANs, and clock data recovery (CDR) circuits [1]–[3].

The design considerations of a VCO include phase noise, tuning range, output power, and chip size. The phase-noise issue of a VCO is becoming more important above the Ku-band due to poor quality factors of integrated *LC* tanks. Despite numerous efforts to increase the quality factor of *LC* tanks, not much attention has been paid to negative g_m cells, which are underrated. The negative g_m cell can be implemented by two different structures mostly in the Ku-band. One is a differential voltage-controlled oscillator (D-VCO) and the other is a balanced voltage-controlled oscillator (B-VCO). The D-VCO is a conventional cross-coupled differential configuration that has been widely adapted in low gigahertz regimes due to its simplicity and differential operation. The D-VCO is immune to the common mode noise generated from active devices, supply, and substrate. On the other hand, the B-VCO is derived from a Colpitts configuration [4]–[7], which has been used in millimeter-wave regimes. In order to take the advantage of common noise rejection, two Colpitts VCOs are balanced to operate with an opposite polarity in the B-VCO [7]–[10]. This can employ the merits of a Colpitts VCO such as high output voltage swing and high-energy efficiency, as well as low common-mode noise.

The two different topologies have been compared [11]–[17]. They offer a little insight into the phase noise of the VCOs. This paper presents the more theoretical analysis, as well as measured results of the negative g_m cell in the two topologies. The analysis with noise models is given in Section II and experiment results are addressed in Section III.

II. VCO Topology Comparison

A. Tank Voltage

The tank voltage of a VCO has a great effect on the phase noise of a VCO as inferred from the phase noise model proposed by Lesson [18] as follows:

$$L(\Delta\omega) = 10 \cdot \log \left\{ kTR_{SL} \frac{F}{V_0^2} \left[\left(\frac{f_0}{Q\Delta f} \right)^2 \right] \right\} \quad (1)$$

where k is the Boltzmann's constant, T is the absolute temperature, R_{SL} is the *LC*-tank resistance at the oscillation frequency (f_0), Δf is the offset frequency, V_0 is the voltage amplitude in the *LC* tank, Q is the quality factor of the tank, and F is the empirical fitting parameter. The phase noise is inversely proportional to the tank amplitude. The amplitude can be increased by an increase of bias current, while active device noise is increased. It is important to make a VCO operate with high tank voltage while minimizing the bias current. The relation between the tank voltage and bias current depends on how to make a negative-conductance cell.

Fig. 1 shows the schematics of the studied D-VCO and B-VCO. All the components used in the two VCOs are identical, except the capacitive feedback methods and tail currents I_T. In the D-VCO, the capacitive feedback from the collector to the base of switching transistors, i.e., Q_1 and Q_2, is used to form positive feedback through C_{f1} and C_{f2}. The feedback capacitor C_{f1} takes a role of dc blocking for the

Manuscript received November 5, 2003; revised November 20, 2003. This work was supported by the Korea Science and Engineering Foundation, Millimeter-Wave Innovation Technology Research Center.

D. Baek, S. Ko, J.-G. Kim, and S. Hong are with the Department of Electrical Engineering and Computer Science, Korea Advanced Institute of Science and Technology, Daejeon 305-701, Korea (e-mail: dhbaek@eeinfo.kaist.ac.kr; schong@ee.kaist.ac.kr).

D.-W. Kim is with the S1 Corporation, Seoul 100-130, Korea (e-mail: xpert.kim@samsung.com).

Digital Object Identifier 10.1109/TMTT.2004.825726

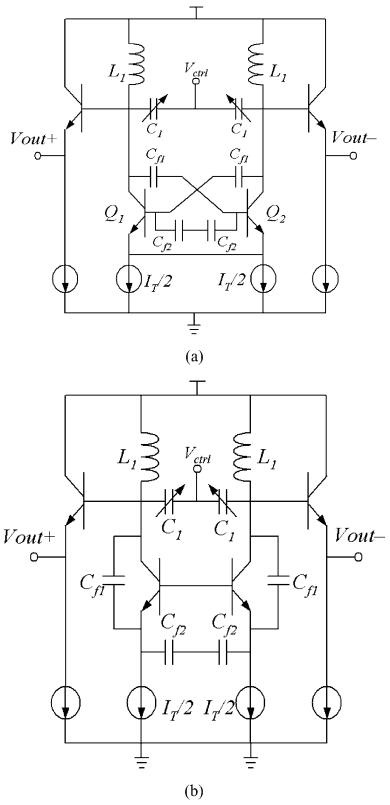

Fig. 1. Schematics of compared topologies of a: (a) D-VCO and (b) B-VCO.

base bias feeding. When the operation frequency is low, the current waveform appears in a rectangular form so that the tank voltage in each collector is $(2/\pi) \cdot I_T \cdot R_{\rm tank}$, where I_T is the tail current and $R_{\rm tank}$ is the resistance of the *LC* tank at the oscillation frequency. However, as the operation frequency increases, the current waveform becomes sine-wave like. Hence, in the Ku-band, the tank amplitude can be written as

$$V_{\rm Tank} = \frac{1}{2} \cdot R_{\rm Tank} I_T. \tag{2}$$

In the B-VCO, the self-capacitive feedback from collector to emitter is used to form a positive feedback due to the same polarity at the collector and emitter voltages. The tank amplitude is determined by the feedback capacitor ratio [19]

$$V_{\rm Tank} = R_{\rm Tank} I_T (1 - n) \tag{3}$$

where n is the capacitance ratio $C_{f1}/(C_{f1} + C_{f2})$. Actually, C_{f2} includes the base–emitter parasitic capacitance. The ratio is nominally approximately 1/4. Considering (2) and (3), the tank voltage of the B-VCO can be larger at the same tail current I_T.

To oscillate a VCO, the magnitude of the negative resistance has to be equal or larger than that of the *LC* tank. To decrease the noise of the transistor or increase the tank amplitude, the g_m cell should have the large negative resistance at a small tail current. To compare the magnitude of negative conductances of the two topologies at the same tail currents, the negative conductance cells are simulated in Agilent ADS, as shown in Fig. 2. The g_m cells are composed of the identical transistors, capacitors, and resistors. The tail currents of the g_m cells are fixed equally under 3-V supply voltage.

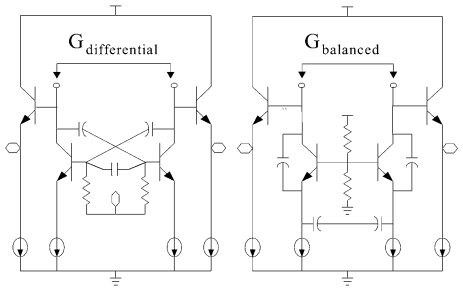

Fig. 2. Negative resistance cells in a differential topology and balanced topology.

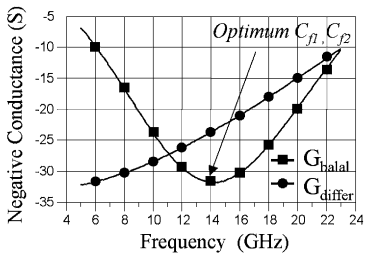

Fig. 3. Simulated negative conductances of the D-VCO (•) and B-VCO (■).

The negative conductance in the balanced topology is much smaller than that in the differential one at low frequency. The differential one is suitable in low frequency. However, the conductance in the balanced topology is larger than that in the differential one above 11 GHz, as shown in Fig. 3. The conductance in the balanced topology is 30% higher than that in the differential topology at the optimum point. Thus, the balanced VCO can oscillate in a lower tail current at the high frequency. The balanced VCO has the larger amplitude in the same tail current than the differential VCO. These coincide with (2) and (3).

B. Noise Analysis

Phase-noise simulations include a nonlinear large-signal model and harmonic-balanced simulation [19]. Although these are available to predict the accurate phase noise, these are too complex to understand the VCO operations and phase noises. The linear phase-noise model is a simple approach that gives good insight into phase noises [17]. The phase-noise performances of two types of VCOs are compared to understand the effects of circuit topologies with a linear model.

In a bipolar junction transistor (BJT) including a heterojunction bipolar transistor (HBT), the physical model has three main noise sources. The first is the base resistance noise $(\overline{v_{nb}^2})$, which is thermal noise. The second is the shot noise from collector current $(\overline{i_{nc}^2})$. The last is shot noise from the base current and flicker noise $(\overline{i_{nb}^2})$ as follows:

$$\begin{aligned} \overline{v_{nb}^2} &= 4kT \cdot r_b \cdot \Delta f \\ \overline{i_{nc}^2} &= 2q \cdot I_c \cdot \Delta f \\ \overline{i_{nb}^2} &= 2q \cdot I_B \cdot \Delta f + K_1 \cdot \frac{I_B^{\alpha}}{f} \cdot \Delta f \end{aligned} \tag{4}$$

where I_s is the base current, I_c is the collector current, r_b is the base resistance, K_I is the flicker noise factor, and α is the flicker noise exponent. All the noises can be thought to be independent

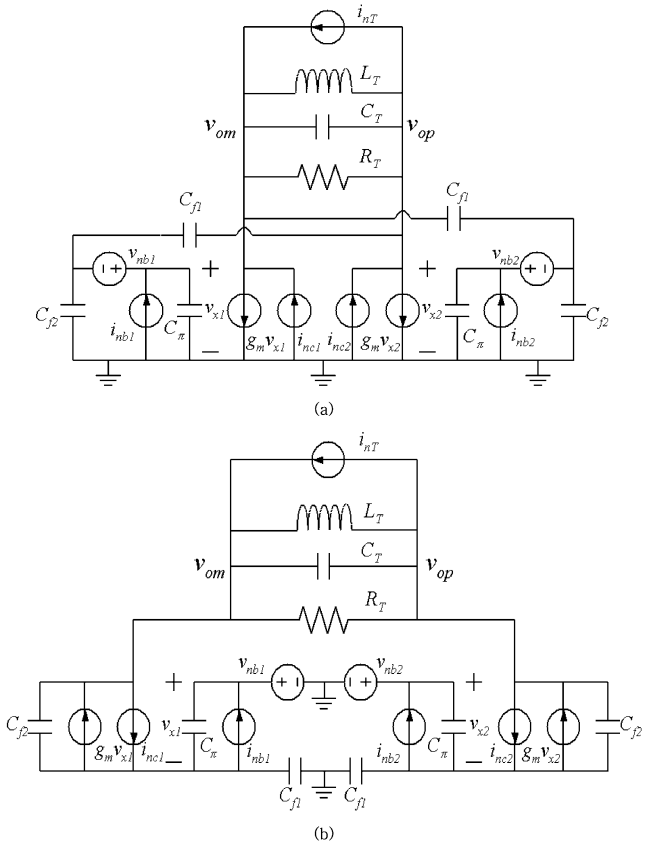

Fig. 4. Equivalent circuits with noise models. (a) D-VCO. (b) B-VCO.

of each other because they arise from spatially separated and independent physical mechanisms [20].

Fig. 4 represents linear models of two different topologies. The transistor model includes the aforementioned noise source. The *LC* tank noise i_{nT} is also included. For simplicity, the collector–base capacitances C_μ, base resistances r_π, and noise from a current source are neglected.

Since these small-signal analyses contain all possible noise sources, the noise in the two types of VCOs can be compared in the linear regime [21]. If the transistors, Q_1 and Q_2 in the differential pair in Fig. 1 are identical, then the differential tank amplitude v_0 is described by the superposition of all the noise sources

$$v_0 = v_{op} - v_{om} = a_1 \cdot i_{nc1,2} + a_2 \cdot i_{nb1,2} + a_3 \cdot v_{nb1,2} + a_4 \cdot i_{nT} \quad (5)$$

where a_1, a_2, a_3, and a_4 indicate the noise contributions coefficients. Since each noise sources are uncorrelated, the total power spectral density is calculated by summing up all the noise powers as follows:

$$\overline{v_o^2} = \frac{1}{2} \cdot \left(2 \cdot a_1^2 \cdot \overline{i_{nc}^2} + 2 \cdot a_2^2 \cdot \overline{i_{nb}^2} + 2 \cdot a_3^2 \cdot \overline{v_{nb}^2} + 2 \cdot a_4^2 \cdot \overline{i_{nT}^2} \right). \quad (6)$$

The factor of "2" in each term inside the parentheses accounts for the differential nature of the circuit. The factor of "1/2" outside the parentheses is due to the noise transfer.

The tank amplitude of the differential topology is derived from the linear model, as shown in Fig. 4(a), and as follows:

$$\begin{aligned} v_{od} &= v_{op} - v_{om} \\ &= \frac{1}{2} s L_T \left[i_{nc1,2} - \frac{g_m + sC_{f1}}{sC_\sigma} \cdot i_{nb1,2} + \left\{ \frac{C_\pi}{C_\sigma} (g_m + sC_{f1}) - g_m \right\} \cdot v_{nb1,2} + 2 \cdot i_{nT} \right] \end{aligned} \quad (7)$$

where

$$\begin{aligned} D_d(s) &= 1 - \left(\frac{C_{f1} g_m}{2C_\sigma} - \frac{1}{R_T} \right) s L_T + L_T C_{\text{eff}} s^2 \\ C_{\text{eff}} &= C_T + \frac{C_{f1}(C_{f2} + C_\pi)}{2C_\sigma} \\ C_\sigma &= C_{f1} + C_{f2} + C_\pi. \end{aligned} \quad (8)$$

At frequencies close to the oscillation frequency $\omega_0 = 1/\sqrt{L_T C_{\text{eff}}}$, the denominator in (7) is close to zero. Since the second term in $D_d(s)$ approaches zero at steady oscillation state, g_m is represented by

$$g_m = \frac{2C_\sigma}{C_{f1}} \cdot \frac{1}{R_T}. \quad (9)$$

Even if $g_m \gg 1$ at the open loop, $g_m \ll 1$ at the steady state because $C_{f1}/C_\sigma = n \approx 1/4$ and $R_r \gg 1$.

In the same manner, the tank amplitude of the balanced topology is derived from the linear model as shown in Fig. 4(b), and as follows:

$$\begin{aligned} v_{ob} &= v_{op} - v_{om} \\ &= \frac{1}{2} s L_T \left[\frac{s(C_{f2} + C_\pi)}{sC_\sigma + g_m} \cdot i_{nc1,2} - \frac{g_m + sC_{f1}}{g_m + sC_\sigma} \cdot i_{nb1,2} + \frac{C_\pi}{C_\sigma} \left(- \frac{g_m s C_2 - s^2 C_{f1} C_\pi}{g_m + sC_{f2}} \right) \cdot v_{nb1,2} + 2 \cdot i_{nT} \right] \end{aligned} \quad (10)$$

where

$$D_b(S) = 1 + \frac{sL_T}{R_T} + s^2 L_T \left(C_T + \frac{C_{f1}}{2} \right) - \frac{s^2 L_T C_{f2}}{2} \frac{sC_{f1} + g_m}{sC_\sigma + gm}. \quad (11)$$

At the steady state, $g_m \ll 1$ is satisfied due to (9). Under this condition, (10) is simplified as

$$\begin{aligned} v_{ob} &= v_{op} - v_{om} \\ &= \frac{\frac{1}{2} s L_T}{D_b(s)} \left[\frac{C_{f2} + C_\pi}{C_\sigma} \cdot i_{nc1,2} - \frac{g_m + sC_{f1}}{sC_\sigma} \cdot i_{nb1,2} + \frac{C_\pi}{C_\sigma} \left(g_m - \frac{sC_{f1} C_\pi}{C_{f2}} \right) \cdot v_{nb1,2} + 2 \cdot i_{nT} \right] \end{aligned} \quad (12)$$

and the denominator $D_b(s)$ become the same as $D_d(s)$ as follows:

$$D_b(s) = 1 - \left(\frac{C_{f1}g_m}{2C_\sigma} - \frac{1}{R_T}\right) sL_T + L_T C_{\text{eff}} s^2. \quad (13)$$

When the oscillation frequency and bias current are identical in both the D-VCO and B-VCO, noise contributions from all the noise sources can be compared for both VCOs noting (7) and (12). The ratio of the noise power from the collector current noise is given by

$$\frac{a_1^2 \text{ of } \overline{v_{ob}^2}}{a_1^2 \text{ of } \overline{v_{od}^2}} = \left(1 - \frac{\omega_0 C_{f1}}{\omega_0 C_\sigma}\right)^2 = (1-n)^2$$

from

$$\overline{i_{nc}^2} = 2qI_c. \quad (14)$$

This is simplified into a function of feedback capacitance ratio n. The tank current in the B-VCO supply charges to C_{f1}. Since the charge in C_{f1} is increased as n is increased, the contribution of a collector current noise is also decreased and the phase noise in the B-VCO can be lowered as compared to the D-VCO. However, the value of n is limited by $n \cdot V_{\text{Tank}} < V_{\text{BE}}$.

The noise powers attributed to the tank noise, and the base current and voltage noises are compared in (15)–(17) as follows:

$$\frac{a_2^2 \text{ of } \overline{v_{ob}^2}}{a_2^2 \text{ of } \overline{v_{od}^2}} = \left(\frac{g_m + sC_{f1}}{g_m + sC_{f1}}\right)^2 = 1$$

from

$$\overline{i_{nb}^2} = 2qI_B + K_1 \frac{I_B}{f} \quad (15)$$

$$\frac{a_3^2 \text{ of } \overline{v_{ob}^2}}{a_3^2 \text{ of } \overline{v_{od}^2}} = \left(\frac{g_m C_{f2} - sC_{f1}C_\pi}{g_m(C_{f1}+C_{f2}) - sC_{f1}C_\pi}\right)^2 \approx 1$$

from

$$\overline{v_{nb}^2} = 4kTr_b \quad (16)$$

$$\frac{a_4^2 \text{ of } \overline{v_{ob}^2}}{a_4^2 \text{ of } \overline{v_{od}^2}} = \left(\frac{2}{2}\right)^2 = 1$$

from

$$\overline{i_{nT}^2} = \frac{4kT}{R_T}. \quad (17)$$

The noise contribution ratios from other noises are calculated in (15)–(17). It is found that there is no topological advantage in the comparisons for base current noise, flicker noise, base voltage noise, and tank noise. It also has to be noted that most of the noise power is attributed to collector current noise. The B-VCO is more immune to active device noises.

III. Experimental Results

A D-VCO and B-VCO are designed and implemented and fabricated on an InGaP–GaAs HBT technology, which offers the n-p-n HBTs with an f_T of 10 GHz and an $f_{\max}$ of 45 GHz. The turn-on voltage of the HBT is 1.3 V. The current density of the HBT is 0.2 mA/μm^2. 60-μm^2 emitter size transistors are used. The technology provides a nitride metal–insulator–metal (MIM) capacitor, a TaN register, and two metal layers, of which thickness are 1 and 1.3 μm. Microstrip lines as inductors are implemented connecting two metal layers. Junction capacitances between the collector and base in transistors are used for frequency tuning. The layout was made as symmetric as possible to ensure truly differential operation. Photographs of the fabricated VCOs are shown in Fig. 5.

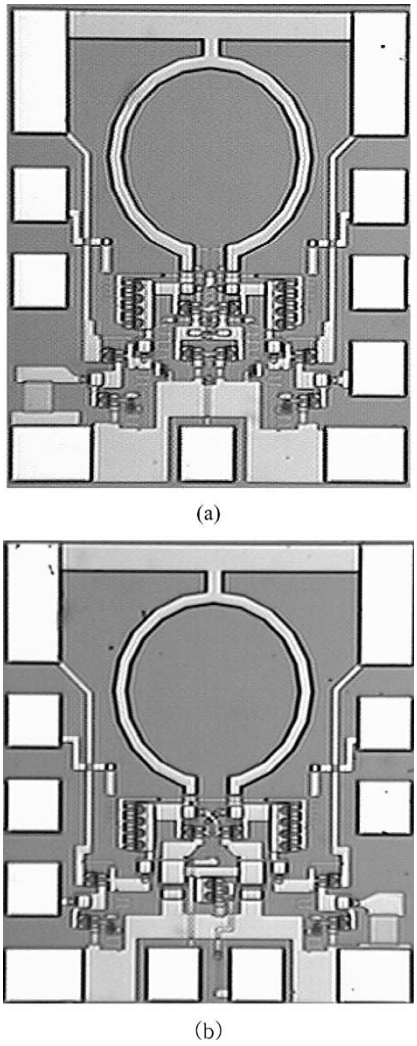

Fig. 5. Microphotographs of the: (a) D-VCO and (b) B-VCO. The dimensions are 0.7 × 0.82 mm^2 in each VCO.

The VCOs was tested on on-wafer. The output spectrums and phase-noise performance were obtained by an HP8764E spectrum analyzer and the phase-noise measurement kit. The cable loss including a probe tip in measurement setup is approximately 2 dB at 13 GHz. The oscillation frequency of the B-VCO is higher than that of the D-VCO because the capacitance in the collector–base junction of the negative conductance cell lowers the tank resonance frequency in the D-VCO. The oscillation frequencies are 12.3 and 13.5 GHz, respectively. The B-VCO provides high output power of 0 dBm per side with the core current of 12 mA and the buffer current of 12 mA. While the D-VCO shows the lower power of approximately −1.5 dBm with a 16-mA core current and 12-mA buffer current. The core current is controlled by the external bias and is optimized for low phase-noise performance. The tank voltage inferred from

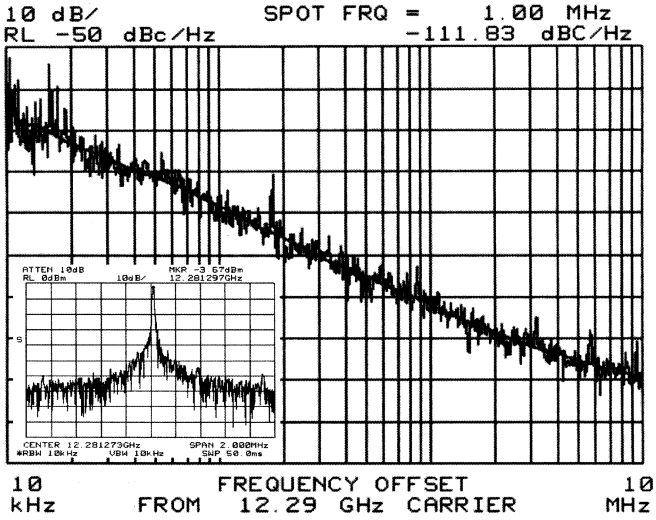

Fig. 6. Phase-noise and output spectrums of the D-VCO at the lowest tuning voltage.

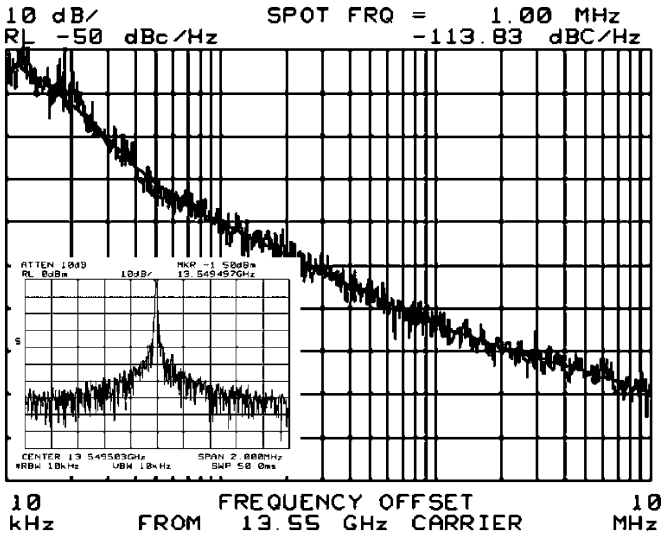

Fig. 7. Phase-noise and output spectrums of the B-VCO at the lowest tuning voltage.

the output power is higher in the B-VCO, although the D-VCO core circuits consume more current than that of the B-VCOs. It reveals that, in the Ku-band, the balanced topology can gives larger negative conductance than the conventional differential topology.

The single-sideband carrier-to-phase-noise ratio (SSCR) of the D-VCO at the lowest tuning voltage are -88 and -111.8 dBc/Hz at 100 kHz and 1 MHz off carrier, as shown in Fig. 6. The SCCRs of the B-VCO at the lowest of tuning voltages show 2–3 dB better and are 90.5 and -113.8 dBc at 100 kHz and 1 MHz off carrier, as shown in Fig. 7.

The tuning ranges are 600 and 800 MHz for the D-VCO and B-VCO, respectively, as shown in Fig. 8. Output power variations are less than 1 dB with the varactor control bias from 0 to 2.5 V for both VCOs. Even though the core current of the B-VCO is small, output power of the B-VCO is approximately 1.5 dB larger than that of D-VCO. This coincides with the theoretical analysis in Section II. The tuning range of the B-VCO

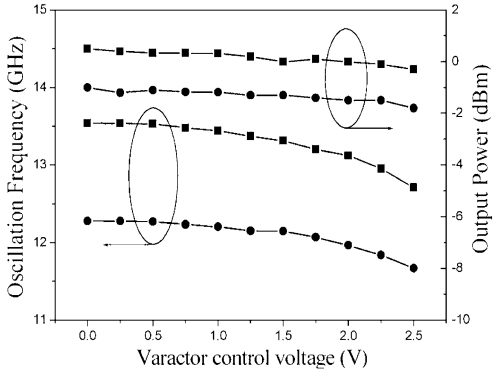

Fig. 8. Measured oscillation frequencies and single-sideband output powers of the D-VCO (•) and B-VCO (■) as a function of the varactor control bias.

TABLE I
SUMMARY OF PERFORMANCES FOR THE BALANCED AND DIFFERENTIAL VCOs

VCO	Balanced	Differential
Frequency (GHz)	12.71-13.54	11.71-12.28
Bias (V)	3 V	3 V
Output power (dBm)	~ 0 (single out)	~ -1.5(single out)
I_{core} & I_{buffer} (mA)	12, 12 each	16,12 each
P_{diss} in core (mW)	36	48
Phase noise @100 kHz	-90.5 dBc/Hz	-88 dBc/Hz
Phase noise @1 MHz	-113.8 dBc/Hz	-111.8 dBc/Hz
Tuning range (MHz)	800	600
F.O.M (dB)	-180.7	-176.6
Size of chip (mm^2)	0.7 X 0.82	0.7 X 0.82

is larger than that of the D-VCO even though all components in both VCOs are identical. This is because the bias current in the B-VCO is low and the parasitics of the B-VCOs transistors is smaller than that of D-VCO. Due to small parasitics, the oscillation frequency of the B-VCO is also higher than that of D-VCO. The VCO performances are summarized in Table I.

IV. DISCUSSION

The main difference of the D-VCO and B-VCO is the capacitive-feedback mechanism, as shown in Fig. 1. Even though the feedback factors and all components are the same, the phase noises, as well as the negative conductance of two VCOs, are different.

In Section II, two merits of the B-VCO are compared with the D-VCO.

One is the high tank voltage, which comes from high negative conductance in the negative g_m cell. The tank amplitudes are expressed in (2) and (3). In our VCO designs, n is set to be 1/4. By comparing two equations at the same tank voltage, the D-VCO requires approximately a 30% higher tail current than the B-VCO with the same bias current. This coincides with the simulation results in Fig. 3.

The other is low noise contribution in the resonator. It needs a larger current until the tank voltage swing reaches a voltage-limited regime compared to the B-VCO since higher tail current

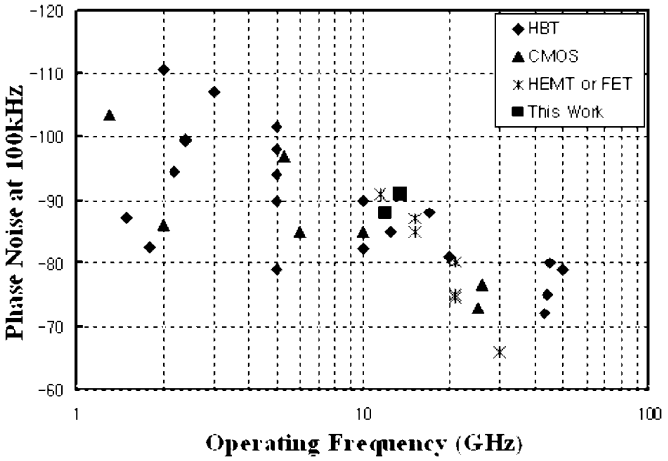

Fig. 9. Comparison of phase noise at 100-kHz offset with the other VCOs in the literature.

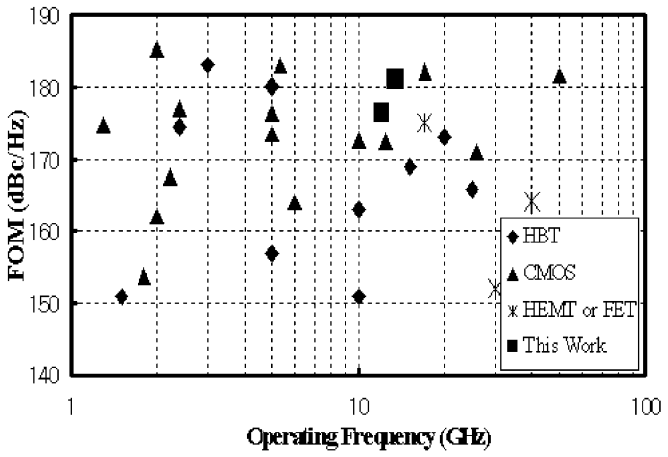

Fig. 10. FOM comparison with ever-reported VCOs. The balanced and differential VCOs exploiting a microstrip-line inductor show -181 and -176 dBc/Hz.

is accompanied by high noise current, which is up-converted near the carrier frequency. Even though transistor noises are identical, the shot noise of the collector current is reduced by the feedback ratio n in the B-VCO. Thereby, the D-VCO has the higher phase noise. For comparison, the phase-noise performances of other VCOs realized on the different technologies are plotted in Fig. 9.

Aparicio and Hajimiri [8] compare the effective impulse sensitivity functions (ISFs) of the D-VCO and B-VCO using cyclostationary noise properties. They address that the effective ISF of the conventional D-VCO is more nonsymmetrical than that of the B-VCO, therefore, the B-VCO has better phase noise performance than the D-VCO.

To decrease the phase noise, the higher tank amplitude and lower noise contributions from transistors are needed. The linear noise model in Section II cannot explain the cyclostationary noise, but it can give good insight into the tank amplitude and noise contributions. It is expected in Section II that the phase-noise performance of the B-VCO is superior to that of the D-VCO. This coincides with the experiment results in Section III.

It is not easy to compare the performance of different VCOs. The oscillator design entails consideration of phase noise, power consumption, oscillation frequency, tuning range, etc. The widely used definition of the normalized figure-of-merit (FOM) is [22] as follows:

$$\mathrm{FOM} = \left(\frac{f_{\mathrm{osc}}}{f_m}\right)^2 \frac{1}{\Lambda_{\mathrm{meas}}(f_m) \cdot P_{\mathrm{diss}}} \tag{18}$$

where f_{osc} is an oscillation frequency, f_m is an offset frequency, Λ_{meas} is the measured phase noise, and P_{diss} is the power consumption in a VCO core. Although it does not include any information about the tuning range and output power, it gives good comparative insights into the VCO performances.

The FOM of the B-VCO and D-VCO is 181 and 177 dB, respectively. The FOM of the B-VCO is 4 dB higher than that of the D-VCO when all components of two VCOs are identical. It is better or comparable to the state-of-art VCOs implemented on CMOS or SiGe HBT technologies, as shown Fig. 10.

V. Conclusion

Noise performances of the balanced and differential VCOs have been studied using analytical noise models. This shows that the B-VCO gives higher tank voltage at the same tail current and has higher immunity to the noise sources of active devices. It has also been determined that the collector-current–noise contribution on the output signal can be diminished by increasing the voltage feedback ratio in the B-VCO.

Two types of Ku-band VCOs are realized on the InGaP–GaAs HBT technology. The B-VCO has shown lower phase-noise performance than the differential VCO, as expected in the noise analysis. The B-VCO and D-VCO achieve the phase noise of -113.8 and -111.8 dBc at the offset frequencies of 1 MHz from the oscillation frequency of 13.5 and 12.55 GHz, respectively. This coincides with the theoretical analysis that the phase-noise performance of the B-VCO is superior to that of the D-VCO at the same tail current.

Acknowledgment

The authors would like to thank the staffs of TELTRON, Daejeon, Korea, for the chip fabrication and support.

References

[1] B. H. Klepser, M. Scholz, and W. Klein, "A 10 GHz SiGe BiCMOS phase-locked-loop frequency synthesizer," in *IEEE Custom Integrated Circuits Conf.*, 2001, pp. 567–570.

[2] Y. M. Greshishchev and P. Schvan, "SiGe clock and data recovery IC with linear-type PLL for 10-Gb/s SONET application," *IEEE J. Solid-State Circuits*, vol. 35, pp. 1353–1359, Sept. 2000.

[3] C. Lam and B. Razavi, "A 2.6 GHz/5.2 GHz frequency synthesizer in 0.4 μm CMOS technology," *IEEE J. Solid-State Circuits*, vol. 35, pp. 788–794, May 2000.

[4] H. Kuhnert and W. Heinrich, "25 GHz MMIC oscillators on a commercial SiGe process," *Electron. Lett.*, vol. 36, no. 3, pp. 218–219, Feb. 2000.

[5] P. J. Garner, M. J. Howes, and C. M. Snowden, "Ka-band and MMIC pHEMT-based VCOs with low phase-noise properties," *IEEE Trans. Microwave Theory Tech.*, vol. 46, pp. 1531–1536, Oct. 1998.

[6] C. H. Lee, S. Han, B. Matinpour, and J. Laskar, "A low phase noise X-band MMIC GaAs MESFET VCO," *IEEE Microwave Guided Wave Lett.*, vol. 10, pp. 325–327, Aug. 2000.

[7] S. P. Voinigescu, D. Marchesan, and M. A. Copeland, "A family of monolithic inductor–varactor SiGe HBT VCOs for 20 GHz to 30 GHz LMDS and fiber optic receiver applications," in *IEEE RF Integrated Circuits Symp.*, 2000, pp. 173–176.
[8] R. Aparicio and A. Hajimiri, "A noise-shifting differential Colpitts VCO," *IEEE J. Solid-State Circuits*, vol. 37, pp. 1728–1736, Dec. 2002.
[9] W. M. Rogers, J. A. Macedo, and C. Plett, "The effect of varactor nonlinearity on the phase noise of completely integrated VCOs," *IEEE J. Solid-State Circuits*, vol. 35, pp. 1360–1366, Sept. 2000.
[10] D. H. Baek, J. G. Kim, and S. Hong, "Ku-band InGaP/GaAs HBT MMIC VCOs with a balanced and a differential topologies," in *IEEE MTT-S Int. Microwave Symp. Dig.*, Seattle, WA, 2002, Paper WE2D-5, pp. 847–850.
[11] H. Jacobbson, S. Gevorgian, M. Mokhtari, C. Hedenas, B. Handsson, T. Lewin, H. Berg, W. Rabe, and A. Schuppen, "Low phase noise low power IC VCOs for 5–8 GHz wireless application," *IEEE Trans. Microwave Theory Tech.*, vol. 48, pp. 2533–2539, Dec. 2000.
[12] C. M. Hung, B. A. Floyd, B. Park, and K. K. O, "Fully integrated 5.35-GHz CMOS VCOs and prescalers," *IEEE Trans. Microwave Theory Tech.*, vol. 49, pp. 17–22, Jan. 2001.
[13] S. Jansen, K. Negus, and D. Lee, "Silicon bipolar VCO family for 1.1 to 2.2 GHz with fully-integrated tank and tuning circuits," in *IEEE Solid-State Conf.*, 1997, pp. 392–393.
[14] E. Hegazi, H. Sjoland, and A. A. Abidi, "A filtering technique to lower *LC* oscillator phase noise," *IEEE. J. Solid-State Circuits*, vol. 36, pp. 1921–1930, Dec. 2001.
[15] J. Plouchart, H. Ainspan, M. Soyer, and A. Ruehli, "A fully-monolithic SiGe differential voltage controlled oscillator for 5 GHz wireless applications," in *IEEE RF Integrated Circuits Symp.*, 2000, pp. 57–60.
[16] F. Herzel, M. Pierschel, P. Weger, and M. Tiebout, "Phase noise in a differential CMOS voltage-controlled oscillator for RF applications," *IEEE Trans. Circuits Syst. II*, vol. 47, pp. 11–15, Jan. 2000.
[17] B. Razavi, "A study of phase noise in CMOS oscillators," *IEEE. J. Solid-State Circuits*, vol. 31, pp. 331–343, Mar. 1996.
[18] D. B. Lesson, "A simple model of feedback oscillator noise spectrum," *Proc. IEEE*, vol. 54, pp. 329–330, Feb. 1966.
[19] A. Hajimiri and T. H. Lee, *The Design of Low Noise Oscillators*. Norwell, MA: Kluwer, 1999.
[20] P. Gray and R. G. Meyer, *Analysis and Design of Analog Integrated Circuits*, 3rd ed. New York: Wiley, 1993.
[21] A. Niknejad and R. Meyer, *Design, Simulation and Applications of Inductors and Transformers for Si RF ICs*. Norwell, MA: Kluwer, 2000.
[22] R. Aparicio and A. Hajimiri, "A noise-shifting differential Colpitts VCO," in *IEEE Solid-State Conf.*, 1997, pp. 392–393.
[23] J. Plouchart, H. Ainspan, M. Soyuer, and A. Ruehli, "A fully-monolithic SiGe differential voltage-controlled oscillator for 5 GHz wireless applications," in *IEEE RF Integrated Circuits Symp.*, June 2000, pp. 57–60.

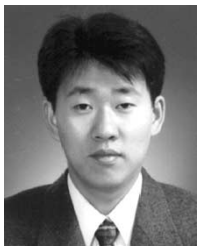

Donghyun Baek (S'98) was born in Chechon, Korea, in 1973. He received the B.S. and M.S. degrees in electrical engineering from the Korea Advanced Institute of Science and Technology (KAIST), Daejon, Korea, in 1996 and 1998, respectively, and is currently working toward the Ph.D. degree at KAIST.

His research interests include high-frequency VCOs, frequency synthesizers, and linear power amplifiers.

Sangsoo Ko (S'02) was born in Iksan, Korea, in 1976. He received the B.S. and M.S. degrees in electrical engineering from the Korea Advanced Institute of Science and Technology (KAIST), Daejon, Korea, in 1994 and 1996, respectively, and is currently working toward the Ph.D. degree at KAIST.

His research interests include high-frequency VCOs, frequency synthesizers, and clock and data recovery circuits.

Jeong-Geun Kim (S'01) received the B.S. and the M.S. degree in electrical engineering from the Korea Advanced Institute of Science and Technology, Daejon, Korea, in 2000 and 2002, respectively, and is currently working toward the Ph.D. degree in millimeter-wave power amplifier design at KAIST.

His research interest includes Gunn diode oscillators, antennas, local multipoint distribution system (LMDS) systems, and power amplifiers.

Dong-Wook Kim received the B.S. degree in electronic communications engineering from the HanYang University, Seoul, Korea, in 1990, and the M.S. and Ph.D. degrees in electrical engineering from the Korea Advanced Institute of Science and Technology (KAIST), Taejeon, Korea, in 1992 and 1996, respectively.

From 1991 to 2000, he was a Member of Technical Staff with the LG Electronics Institute of Technology, Seoul, Korea, where he was involved with the development of microwave and millimeter-wave circuits and modules. From 2000 to 2002, he was a Principal Engineer and General Manager of Telephus Inc., where he led the Product Development Division in the development of Si integrated passive devices and multichip modules for microwave and millimeter-wave applications. In September 2002, he joined the S1 Corporation (a company of the Samsung Group), Seoul, Korea, where he has been involved in the development of wireless security systems. His areas of interest are low-cost passive integration technology, RF and millimeter-wave integrated-circuit design, multichip modules based on low-cost passive integration processes, system-in-a-package, microwave sensors, and wireless systems for security applications.

Dr. Kim is a member of the International Microelectronics and Packaging Society (IMAPS).

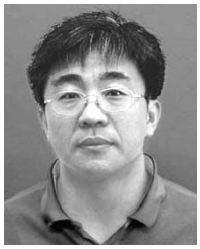

Songcheol Hong (S'87–M'88) received the B.S. and M.S. degrees in electronics from the Seoul National University, Seoul, Korea, in 1982 and 1984, respectively, and the Ph.D. degree in electrical engineering from The University of Michigan at Ann Arbor, in 1989.

In May 1989, he joined the faulty of the Department of Electrical Engineering and Computer Science, Korea Advanced Institute of Science and Technology (KAIST), Daejeon, Korea, as an Assistant Professor, and then became an Associate Professor in 1994 and Professor in 1999. He held short visiting professorships with Stanford University, Stanford, CA, and Samsung Microwave Semiconductor Inc., Milpitas, CA, in 1997. His research interests are microwave integrated circuits including power amplifiers, VCOs, phase-locked loops (PLLs), and frequency synthesizers, as well as opto-electronic devices such as quantum dot infrared detectors and optical modulators. He was recipient, along with his students, of the Third Place Student Paper Award presented at the 2000 IEEE Microwave Theory and Techniques Society (IEEE MTT-S) International Microwave Symposium (IMS) concerning the topic of microelectromechanical system (MEMS) switches. He was also the recipient of the Best Paper (Gold Prize) of the 1998 Samsung Humantech Thesis Prize concerning the topic of quantum dot infrared detectors.